Acta Polytechnica **62**(6):574–588, 2022
https://doi.org/10.14311/AP.2022.62.0574

Published by the Czech Technical University in Prague

STUDY OF SURFACE ROUGHNESS WITH MHD AND COUPLE STRESS FLUID ON POROUS CURVED ANNULAR PLATES

Salma Alla Baksh*, Hanumagowda Bannihalli Naganagowda

REVA University, School of Applied Sciences, Department of Mathematics, Bangalore-560064, India
* corresponding author: salma.alla@gmail.com

Abstract. The purpose of this article is to examine the effect of surface roughness on porous curved annular plates lubricated with couple stress fluid in the presence of magnetic field. The MHD-Stochastic Reynolds equation is derived using Christensen's stochastic model and applied to predict the squeeze film characteristics of porous curved annular plates. The expressions for squeeze film pressure, load-carrying capacity, and squeeze film time are obtained analytically, the results are discussed for various values of operating parameters, and are plotted graphically. It is found that the squeeze film characteristics of porous curved annular plates are improved using a non-Newtonian fluid in the presence of an external magnetic field. The effect of roughness parameter is to increase (decrease) the squeeze film attributes for azimuthal (radial) roughness configuration as compared to the smooth case. Furthermore, the effect of permeability parameter is to decrease the pressure, load-carrying capacity, and squeeze-film time as compared to the non-porous case.

Keywords: Couple stress fluid, MHD, surface roughness, porous medium, curved annular plates.

1. Introduction

In development of modernised machine equipment, a great attention is being paid to fluids which contain microstructures, such as suspensions, long-chained polymers, and additives. Newtonian fluid is one which does not depend on the dimension of fluid particles and hence such fluids are not a suitable engineering concept. Since non-Newtonian fluid flow cannot be precisely explained by the classical theory of continuum, numerous micro continuum theories have been constructed [1, 2] for explaining the particular behaviour of fluids featuring substructures that have the ability to interpret, pivot, or even distort on their own. Among them, Stoke's theory [3] is the simplest theory. Numerous authors have considered this theory to examine the impact of couple stresses for several kinds of fluid film bearings, for example, Lin [4] presented the sphere-flat plate, Kashinath [5] presented the parallel stepped squeeze films plates and Naduvinamani et al. [6] presented circular stepped plates. These authors have concluded that presence of couple stress fluid increases load and film time as compared to classical case. Recently, the concepts of Magnetohydrodynamics (MHD) in lubrication theory have caught the attention of numerous researchers. Since it is found that by using an electrically conducting fluid, the load-carrying capacity in a bearing can be increased. Many theoretical studies have carried out and detected that the impact of electromagnetic fields on squeeze films is beneficial particularly in the devices which involve high speeds and high external temperature. The hydromagnetic bearings, when compared to solid bearings, possess many advantages with couple stress fluid as lubricant. They are capable to function at high temperatures, and they offer a significant resistance to radioactive radiation. To protect undesirable variation in viscosity with temperature, the use of electrically conducting liquid-metal as lubricant is emphasized. In the occurrence of a magnetic field, many authors presented MHD performance of bearings lubricated with an electrically conducting fluid for smoothness, such as slider bearing by Snyder [7], inclined slider bearing and finite step slider bearing by Hughes [8, 9], parallel plate slider bearing by Kuzma [10], Lin [11] for annular disks, and Lin et al. [12] for curved annular If we compare the results with a non-magnetic case there is an enhancement in film pressure, load and the length of the squeeze film time in presence of a magnetic field. In all the above-mentioned papers, it has been observed that the work is limited only for smooth surfaces.

But practically, even the rough surface is very crucial. Keeping this in mind, few investigators have tried to study the effect of porous medium on the rough surfaces. Nowadays, porous medium is one of areas of interest for many authors in various fields of science and engineering. Porous bearings are found to be advantageous due to its self-lubricating properties, lower costs, and design ease. Thus, the study of porous squeeze-film bearings was based on Darcy model, in which fluid flow through porous matrix obeys Darcy's law and no-slip condition was expected on the film interface. Several authors have examined rough surface for hydrodynamic lubrication using stochastic approaches. For example, the stochastic model for rough surfaces have been recognised by Christensen [13]. Numerous investigators have considered this model to examine the impact of roughness for distinctive bearings along with porous medium, such as Bhat et al. [14] for annular discs, Naduvinamani et

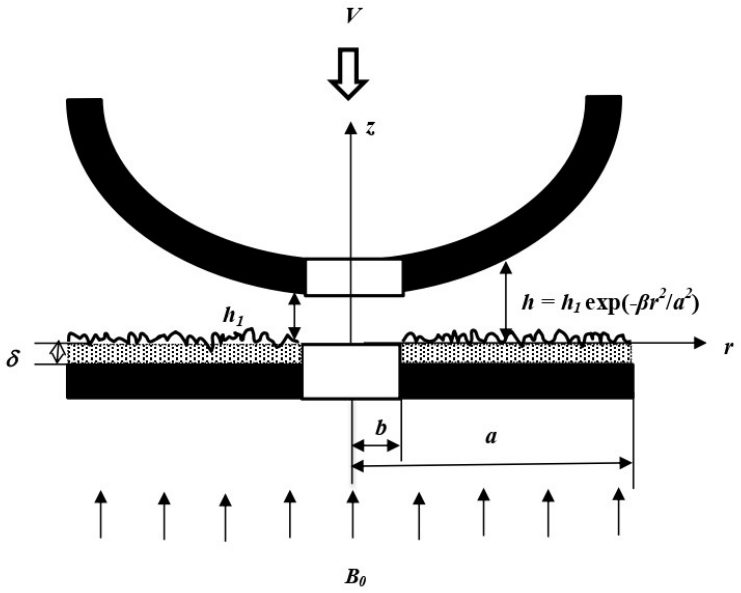

FIGURE 1. Geometry of rough - porous curved annular plates.

al. [15] for circular stepped plates, Syeda et al. [16] for Elliptical Plates, Hanumagowda et al. [17] for circular stepped plates, Biradar et al. [18] for Curved Annular Circular Plates, Hanumagowda et al. [19] for Conical Bearing, Patel et al. [20] for long bearings, Sankar et al. [21] for vertical annulus, Kiran et al. [22] for porous annulus, Shimpi et al. [23] for Curved Porous Annular Plates, and Niru et al. [24] for Curved Porous Annular Plates considering the rotation of magnetic particles and slip velocity. All these authors studied the effect of roughness in presence of porous medium and concluded that the effect of radial (azimuthal) roughness pattern on the bearing surface decrease (increase) the pressure, load carrying capacity, and approach of squeeze film time whereas the permeability parameter decreases these squeeze film attributes as compared to a non-porous case. Motivated by these investigations and their applications, in the present article, the authors examine the combined impact of MHD and surface roughness on the couple stress squeeze film lubrication between curved annular plates by considering the porous medium. The results are analysed for different values of the physical parameters – the pressure, load bearing capacity and squeeze film time. The obtained numerical results for a special case are found to be in good agreement with those of the results available in the literature. Furthermore, the results obtained reveal many interesting behaviours that warrant a further study of the equations related to non-Newtonian couple stress fluid phenomena in the presence of pressure dependent viscosity and slip velocity.

2. Mathematical formulation and solution

The geometry of rough-porous curved annular plates is displayed in Figure 1, having internal radius b and external radius a. The lower plate with permeable facing of thickness δ is fixed while the upper smooth plate is moving with a velocity $V = -dh_1/dt$ towards it. A transverse magnetic field B_0 is applied vertical to the plates.

The shape of the film thickness h is an exponential type as in Jaw-Rein Lin et al. [25]

$$h = h_1 \exp(-\beta r^2/a^2),\ b \le r \le a, \tag{1}$$

where β is the curvature parameter and h_1 is the initial minimum film thickness.

In view of hydrodynamic and hydro-magnetic lubrication, the governing equations, which satisfies Stokes [3] model, are considered as

$$\mu\frac{\partial^2 u}{\partial z^2} - \eta\frac{\partial^4 u}{\partial z^4} - \sigma B_0^2 u = \frac{\partial p}{\partial r}, \tag{2}$$

$$\frac{\partial p}{\partial z} = 0, \tag{3}$$

$$\frac{1}{r}\frac{\partial}{\partial r}(ru) + \frac{\partial w}{\partial z} = 0, \tag{4}$$

in which the components of velocities are u and w in r and z direction, respectively, p represents the pressure in the region, η is the materialistic constant, σ is the electrical conductivity and B_0 is the applied magnetic field.

For the porous region

$$\frac{1}{r}\frac{\partial}{\partial r}(ru^*) + \frac{\partial w^*}{\partial z} = 0. \tag{5}$$

Governing Modified Darcy's equation given by Biradar et al. [26], the velocity components u^* and w^* in porous region are

$$u^* = \frac{-k}{\mu\left(1-\Phi+\frac{kM^2}{mh_0^2}\right)}\frac{\partial p^*}{\partial r}, \tag{6}$$

$$w^* = \frac{-k}{\mu(1-\Phi)}\frac{\partial p^*}{\partial z}, \tag{7}$$

where p^* is the pressure in the porous region, k is the permeability parameter, Φ is the ratio of the microstructure size to pore size, $M = B_0H_0\left(\frac{\sigma}{\mu}\right)^{1/2}$ is the Hartmann number.

The velocity boundary conditions are:

- For lower rough-porous curved annular surface at $z = 0$

$$u = 0,\ \frac{\partial^2 u}{\partial z^2} = 0,\ \text{(Vanishing of couple stresses)} \tag{8a}$$

$$w = 0. \tag{8b}$$

- For upper curved annular surface at $z = h$

$$u = 0,\ \frac{\partial^2 u}{\partial z^2} = 0,\ \text{(Vanishing of couple stresses)} \tag{9a}$$

$$w = V = \frac{-\partial h_1}{\partial t}. \tag{9b}$$

Solving Equation (1) subject to boundary conditions (8a) and (8b), the expression for the velocity component is

$$u = \{(g_1 - g_2) - 1\}\frac{h_0^2}{\mu M^2}\frac{\partial p}{\partial r}. \tag{10}$$

Here,

$$g_1 = g_{11},\ g_2 = g_{12},\ \text{for } 4M^2l^2/h_0^2 < 1 \tag{11a}$$

$$g_1 = g_{21},\ g_2 = g_{22},\ \text{for } 4M^2l^2/h_0^2 = 1 \tag{11b}$$

$$g_1 = g_{31},\ g_2 = g_{32},\ \text{for } 4M^2l^2/h_0^2 > 1 \tag{11c}$$

The associated relations in Equations (11a), (11b) and (11c) are given in Appendix A.

The continuity equation in polar form is obtained by integrating Equation (3) over film thickness using the boundary conditions (8b) and (9b), resulting in

$$\frac{1}{r\mu}\frac{\partial}{\partial r}\left\{rS(h,l,M)\frac{\partial p}{\partial r}\right\} = w_h - w_0, \tag{12}$$

but upper surface is not porous $w_h = 0$.

The velocity component in z-direction is continuous at the interface between the lower plate and film so that

$$w_0 = -\left\{\frac{dh}{dt} + \frac{k}{\mu(1-\Phi)}\left(\frac{\partial p^*}{\partial z}\right)_{z=0}\right\}. \tag{13}$$

By substituting Equation (13) in (12), we obtain

$$\frac{1}{r\mu}\frac{\partial}{\partial r}\left\{rS(h,l,M)\frac{\partial p}{\partial r}\right\} = \frac{dh}{dt} + \frac{k}{\mu(1-\Phi)}\left(\frac{\partial p^*}{\partial z}\right)_{z=0}, \tag{14}$$

where

$$S(h,l,M) = \begin{cases} \frac{h_0^2}{M^2}\left\{\frac{2l}{(A^2-B^2)}\left(\frac{B^2}{A}\tanh\frac{Ah}{2l} - \frac{A^2}{B}\tanh\frac{Bh}{2l}\right) + h\right\} & \text{for } M^2l^2/h_0^2 < 1, \\ \frac{h_0^2}{M^2}\left\{\frac{h}{2}\sec h^2\left(\frac{h}{2\sqrt{2l}}\right) - 3\sqrt{2l}\tanh\left(\frac{h}{2\sqrt{2l}}\right) + h\right\} & \text{for } M^2l^2/h_0^2 = 1, \\ \frac{h_0^2}{M^2}\left\{\frac{2lh_0}{M}\left(\frac{(A_2\cot\theta - B_2)\sin B_2h - (B_2\cot\theta + A_2)\sin A_2h}{\cos B_2h + \cosh A_2h}\right) + h\right\} & \text{for } M^2l^2/h_0^2 > 1. \end{cases}$$

In porous region, fluid pressure satisfies the equation

$$\frac{1}{r}\frac{\partial}{\partial r}\left(r\frac{\partial p^*}{\partial r}\right)+\left(\frac{D}{1-\Phi}\right)\frac{\partial p^*}{\partial z}=0, \tag{15}$$

where $D=\left(1-\Phi+\frac{kM^2}{mh_0^2}\right)$.

Let us integrate the above equation using Morgan-Cameron approximation [27] that is $\frac{\partial p^*}{\partial r}$ at $z=-\delta$ yields,

$$\left(\frac{\partial p^*}{\partial z}\right)_{z=0}=-\left(\frac{1-\Phi}{D}\right)\int_{-\delta}^{0}\frac{1}{r}\frac{\partial}{\partial r}\left(r\frac{\partial p^*}{\partial r}\right)dz.$$

Since porous thickness layer δ is exceedingly small, Morgan-Cameron approximation [27] is considered and Equation (15) yields

$$\left(\frac{\partial p^*}{\partial z}\right)_{z=0}=-\delta\left(\frac{1-\Phi}{D}\right)\frac{1}{r}\frac{\partial}{\partial r}\left(r\frac{\partial p}{\partial r}\right), \tag{16}$$

where $\frac{\partial p^*}{\partial z}=0$ at $z=-\delta$ has been used.

Using Equation (16) in (14) the Reynold's modified equation results in

$$\frac{1}{r\mu}\frac{\partial}{\partial r}\left\{\left(S(h,l,M)+\frac{\delta k}{D}\right)r\frac{\partial p}{\partial r}\right\}=V. \tag{17}$$

According to the stochastic model of Christensen [13], the film thickness H is

$$H=h+h_s(r,\theta,\xi), \tag{18}$$

where h is the nominal thickness, h_s is the part owing to surface roughness as measured from nominal level and ξ is a stochastic variable which describes roughness geometry.

2.1. Stochastic Reynolds equation

Let us take the stochastic mean of Equation (17) with respect to probability density function $g(h_s)$, we get

$$\frac{1}{r\mu}\frac{\partial}{\partial r}\left\{\left(E\left(S(h,l,M)+\frac{\delta k}{D}\right)\right)r\frac{\partial E(p)}{\partial r}\right\}=V, \tag{19}$$

where $E(\bullet)=\int_{-\infty}^{\infty}(\bullet)g(h_s)dh_s$.

The roughness distribution function based on Christensen's theory is in form

$$g(h_s)=\begin{cases}\frac{35}{32n^7}(n^2-h_s^2)^3, & -n<h_s<n\\ 0, & otherwise\end{cases} \tag{20}$$

where $n=3\overline{\sigma}$ and $\overline{\sigma}$ is the standard deviation.

Generally, there are two kinds of roughness configuration, namely:

- **Radial Roughness configuration:** It is one-dimensional roughness in the form of long, narrow ridges and valleys running in r-direction. Film thickness and average modified Reynold's equation is

$$H=h+h_s(\theta,\xi), \tag{21}$$

$$\frac{1}{r\mu}\frac{\partial}{\partial r}\left\langle\left[ES(h,l,M)+\frac{\delta k}{D}\right]r\frac{\partial E(p)}{\partial r}\right\rangle=V, \tag{22}$$

where

$$E(S(h,l,M))=\frac{35}{37n^7}\int_{-n}^{n}S(h,l,M)(n^2-h_s^2)^3dh_s.$$

- **Azimuthal Roughness configuration:** It is one-dimensional roughness in the form of long, narrow ridges and valleys running in θ-direction. Film thickness and average modified Reynold's equation is

$$H=h+h_s(r,\xi), \tag{23}$$

$$\frac{1}{r\mu}\frac{\partial}{\partial r}\left\langle\left([E1/S(h,l,M)]^{-1}+\frac{\delta k}{D}\right)r\frac{\partial E(p)}{\partial r}\right\rangle=V, \tag{24}$$

where

$$E\left(\frac{1}{S(h,l,M)}\right)=\frac{35}{32n^7}\int_{-n}^{n}\frac{(n^2-h_s^2)^3}{S(h,l,M)}dh_s.$$

Introducing the following non-dimensional quantities in Equation (19),

$$r^* = \frac{r}{a},\ h_1^* = \frac{h_1}{h_0},\ h^* = \frac{h}{h_0},\ l^* = \frac{2l}{h_0},\ P = -\frac{h_1^3 p}{\mu a^2 V},\ \delta^* = \frac{\delta}{h_0},\ \Psi = \frac{k\delta}{h_0^3},\ D_1 = \left(1 - \Phi + \frac{\Psi M^2}{m\delta^*}\right),\ C = \frac{n}{h_0}.$$

Here, h_0 is the minimum film thickness.

The modified-stochastic Reynold's equation for film pressure is given by

$$\frac{1}{r^*}\frac{\partial}{\partial r^*}\left\{J(H, l^*, M, \Psi, C) r^* \frac{\partial P}{\partial r^*}\right\} = -1, \tag{25}$$

where

$$J(H, l^*, M, \Psi, C) = \begin{cases} E\left\langle S(h_1^*, l^*, M)\right\rangle + \frac{\Phi}{D_1} & \text{for radial roughness,} \\ \left\langle E\left(1/S(h_1^*, l^*, M)\right)\right\rangle^{-1} + \frac{\Phi}{D_1} & \text{for azimuthal roughness.} \end{cases}$$

The relevant boundary conditions to present the squeeze problem is

$$p = 0 \quad \text{for } r^* = \alpha = b/a, \tag{26a}$$

$$p = 0 \quad \text{for } r^* = 1. \tag{26b}$$

The non-dimensional stochastic Reynold equation (25) is integrated using the boundary conditions (26a) and (26b), which results in the expression for non-dimensional MHD mean squeezing film pressure:

$$p = \frac{f_2(r^*) f_1(1) - f_1(r^*) f_2(1)}{2 f_2(1)}, \tag{27}$$

where

$$f_1(1) = \int_{r^*=\alpha}^{1} \frac{r^*}{J(H, l^*, M, \Psi, C)} dr^*, \quad f_2(1) = \int_{r^*=\alpha}^{1} \frac{1}{r^* J(H, l^*, M, \Psi, C)} dr^*.$$

The pressure field over the plate surface is integrated to find the load supporting capacity and is

$$W = \int_{r=b}^{a} 2\pi r p \, dr. \tag{28}$$

The non-dimensional MHD mean load-supporting capacity W is

$$W = \frac{E(W) h_1^3}{2\pi\mu a^4(-dh_1/dt)} = \frac{-1}{2}\int_{r^*=\alpha}^{1} f_1(r^*) r^* dr^* + \frac{1}{2}\frac{f_1(1)}{f_2(1)}\int_{r^*}^{1} f_2(r^*) r^* dr^*. \tag{29}$$

The non-dimensional squeeze film time for film thickness is

$$T = \frac{E(W) h_1^2}{\pi\mu a^4} t = \int_{h_1^*}^{1} \left(\frac{2 f_2(1)}{f_2(1)\int_{r^*=\alpha}^{1} f_1(r^*) r^* dr^* - f_1(1)\int_{r^*=\alpha}^{1} f_2(r^*) r^* dr^*}\right) dh_1^*. \tag{30}$$

3. Result and discussions

In the present article, the impact of roughness, MHD, and couple stress fluid is investigated. The MHD-Stochastic Reynolds-type equation is derived using Christensen's stochastic model and applied to predict the squeeze film characteristics of porous curved annular plates. The results are discussed for various values of non-dimensional quantities, such as Hartmann number M, couple stress parameter l^*, roughness parameter C, permeability parameter Ψ, curvature parameter β, and radius ratio α. To discuss the squeeze film characteristics, the following parameters range is considered:

$M = 0, 2, 4;\ l^* = 0.0, 0.2, 0.4;\ C = 0.0, 0.2, 0.4;\ \beta = -0.5, 0, 0.5;\ \Psi = 0, 0.001, 0.1;\ \alpha = 0.2, 0.4, 0.6$ and $m = 0.6; \delta^* = 0.01;\ \Phi = 0.2$ are fixed.

Limiting cases:

(i) As $C \to 0$, corresponds to the smooth case discussed by Hanumagowda et al. [28],

(ii) As $C \to 0$, $M \to 0$, corresponds to the non-magnetic case discussed by Gupta et al. [29],

(iii) As $C \to 0$, $M \to 0$, $l^* \to 0$, corresponds to the Newtonian case studied by Jaw et al. [25],

(iv) As $\Psi \to 0$, corresponds to the non-porous case discussed by Hanumagowda et al. [28],

(v) As $\beta = 0$, corresponds to the annular plates discussed by Syeda et al. [30].

3.1. Mean film pressure

Figure 2 presents the profile of mean pressure P along dimensionless co-ordinate axial r^* as a function of C for both roughness configurations and clearly shows that for larger C values, the mean pressure inclines (declines) for azimuthal (radial) roughness structures, and also, when $C \to 0$, it reduces to smooth case. In Figure 3, a graph of P against r^* as a function of Ψ is presented and can clearly be seen that for increasing Ψ values, the mean pressure decreases for azimuthal roughness rather than radial roughness structure. Figure 4 shows the distinctive values of Hartmann number, the graph P against r^* is presented and shows that for increasing M values, the pressure increases. The profile of P against r^* for various l^* values is described in Figure 5 and it can be seen that the impact of l^* is to enhance P. Figure 6 displays the graph of P against r^* for distinctive values of β and it can be seen that the pressure is a significant factor for increasing β values.

3.2. Mean Load supporting capacity

The deviation of mean load supporting capacity W against curvature parameter β as a function of C is displayed in Figure 7 for both roughness configurations and it can be seen that when $C = 0$, an azimuthal and radial roughness configurations coincide and reduce to a smooth case. In Figure 8 the profile of W against β as a function of permeability parameter Ψ is depicted and shows that the mean load declines for larger Ψ values. The graph W along β for several values of Hartmann number is illustrated in Figure 9 and for distinct values of l^* in Figure 10. It is found that the impact of couple stress fluid in the existence of applied magnetic field is to substantially enhance the load supporting capacity as compared to Newtonian fluids. This is due to the use of magnetic field normal to the flow, which results in a lower velocity of the lubricant in the fluid film region. Thus, a large amount of the fluid is retained in the film region, and this yields a rise in pressure. Figure 11 represents the load profile W along β for distinct values of radius ratio α for both roughness configurations and it shows that the mean load decreases for rising values of α. Furthermore, the mean load increases for larger β values.

3.3. Squeeze film time

Figure 12 shows the deviation of dimensionless squeeze film T against dimensionless film height h_1^* for distinct values of C, illustrated for both roughness configurations. From the results obtained, squeeze film time T is predicted to increase (decreases) for azimuthal (radial) roughness configurations as compared to the solid case. The time profile T against h_1^* for distinct values of Ψ is presented in Figure 13 and it clearly shows that T increases for decreasing Ψ values, even more significantly for the azimuthal roughness structure. Figure 14 depict the time variation T against h_1^* as a function of Hartmann number M and shows that T increases for larger M values.

The graph of T against h_1^* for various values of couple stress parameter l^* is shown in Figure 15 and it can clearly be seen that the impact of l^* enhances the squeeze film time. Figure 16 represents the deviation of T against h_1^* for distinct values of radius ratio α and shows that T decreases for larger values of radius ratio. The time profile T along h_1^* as a function of curvature parameter β is illustrated in Figure 17 and shows that for increasing β values, T also increases.

4. Conclusion

Using a stochastic model of Christensen for rough surfaces, the present analysis predicts the influence of roughness on squeeze film attributes for porous annular plates with MHD and couple stress fluid. Through the above discussions, conclusions are drawn as follows:

- The surface roughness impact increases the pressure, load supporting capacity and prolongs film time in comparison with the smooth case. This impact is greater for the azimuthal roughness than the radial roughness structure.
- In a comparison with non-magnetic case, the impact of Hartmann number enhances the squeezing attributes for both roughness structures.
- The couple stress effects for azimuthal roughness are more pronounced than for the radial. Also, the squeeze film attributes are very significant for non-Newtonian case.
- The permeability parameter effect reduces the performance of squeeze-film characteristics as compared to the solid case.
- The load and film time are reduced due to an increase in radius ratio.
- Obtained results are compared with previous analysis carried out by Hanumagowda et al. [28] and shown in the Table 1. It is observed that there is a substantial increase in load and time for both roughness configurations in the porous region. An increase of 14 % (15 %) in radial (azimuthal) roughness configuration is observed when $M = 6$, $C = 0.2$ and $\Psi = 0.001$.
- It is anticipated that these results will help the design engineers in choosing the most suitable structure, magnetic field, and lubricant additives to prolong the bearing's life. These results are in agreement with the experimental study by Artur et al. [31] that the final composition of the lubricant should be supplemented with suitably selected additives.

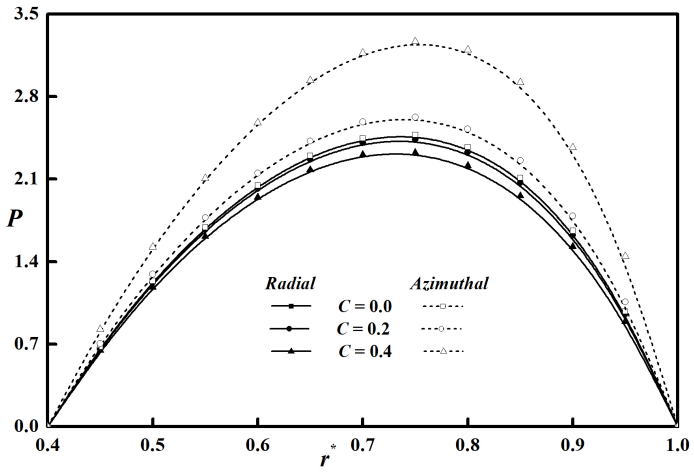

Figure 2. Variation of P against r^* for distinct values of C with $M = 3$, $l^* = 0.3$, $\alpha = 0.4$, $\beta = 0.5$, $\Psi = 0.001$, $m = 0.6$, $\delta^* = 0.01$, $\Phi = 0.2$.

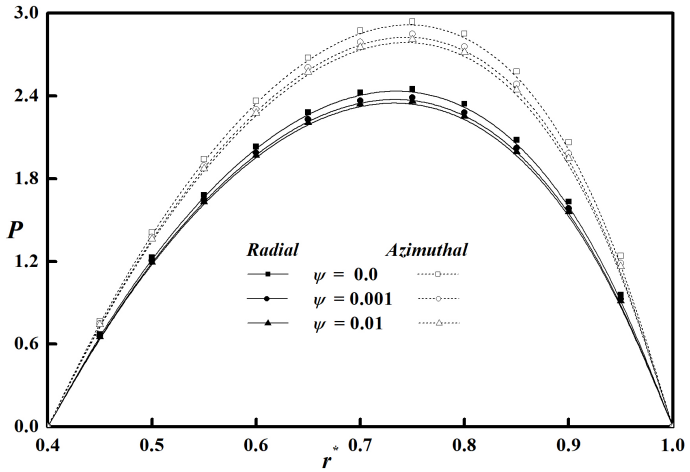

Figure 3. Variation of P against r^* for distinct values of Ψ with $M = 3$, $l^* = 0.3$, $C = 0.3$, $\alpha = 0.4$, $\beta = 0.5$, , $m = 0.6$, $\delta^* = 0.01$, $\Phi = 0.2$.

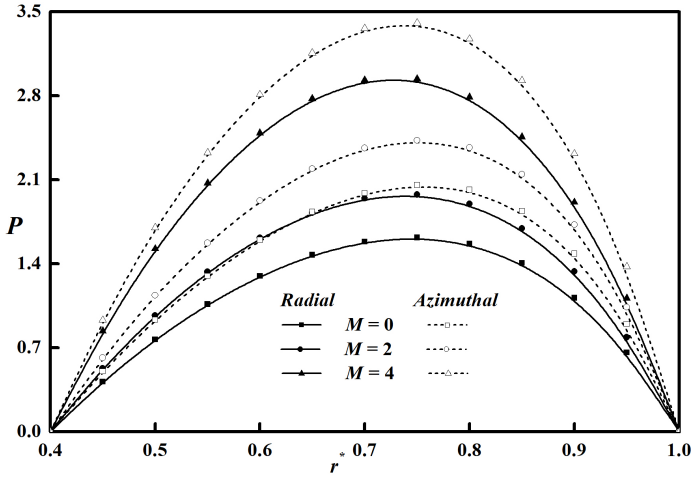

Figure 4. Variation of P against r^* for distinct values of M with $C = 0.3$, $l^* = 0.3$, $\alpha = 0.4$, $\beta = 0.5$, $\Psi = 0.001$, $m = 0.6$, $\delta^* = 0.01$, $\Phi = 0.2$.

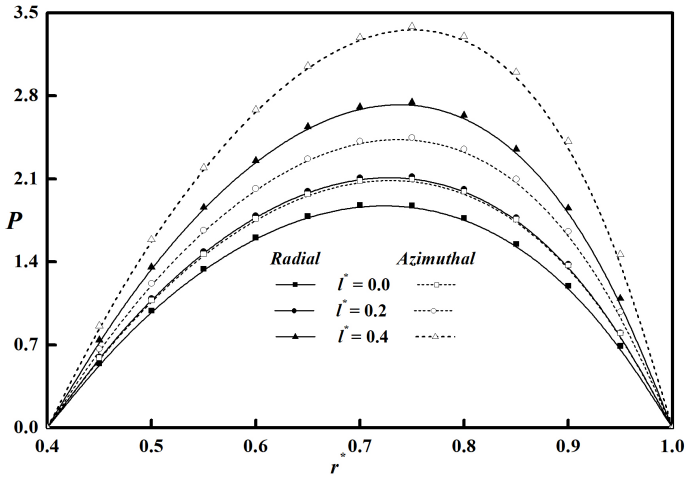

FIGURE 5. Variation of P against r^* for distinct values of l^* with $C = 0.3$, $M = 3$, $\alpha = 0.4$, $\beta = 0.5$, $\Psi = 0.001$, $m = 0.6$, $\delta^* = 0.01$, $\Phi = 0.2$.

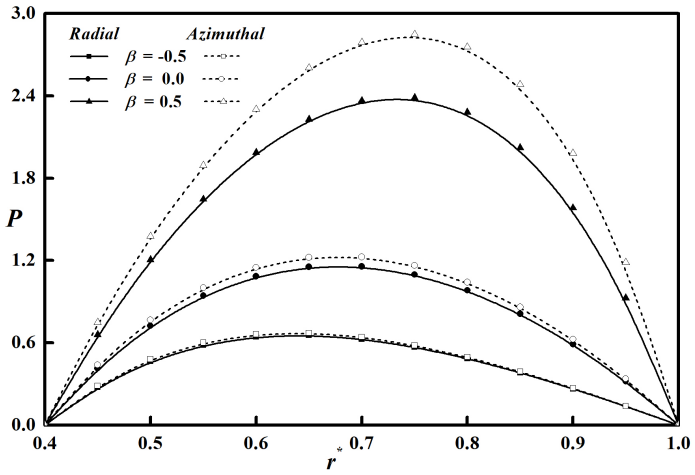

FIGURE 6. Variation of P against r^* for distinct values of β with $C = 0.3$, $M = 3$, $\alpha = 0.4$, $l^* = 0.3$, $\Psi = 0.001$, $m = 0.6$, $\delta^* = 0.01$, $\Phi = 0.2$.

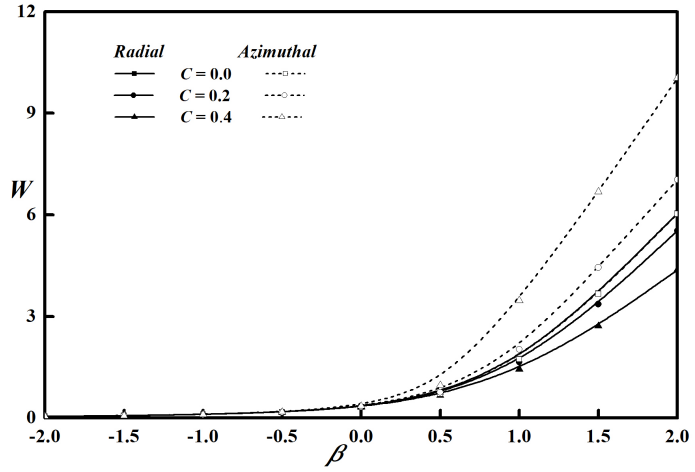

FIGURE 7. Variation of W against β for various values of C with $M = 3$, $l^* = 0.3$, $\alpha = 0.4$, $\Psi = 0.001$, $m = 0.6$, $\delta^* = 0.01$, $\Phi = 0.2$.

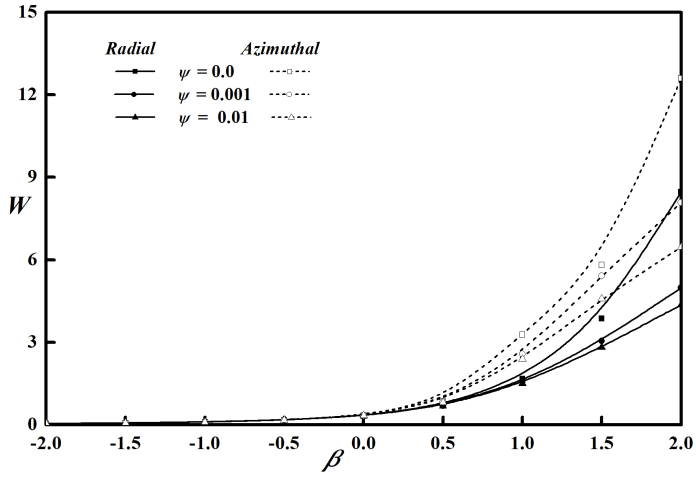

Figure 8. Variation of W against β for various values of Ψ with $M = 3$, $l^* = 0.3$, $C = 0.3$ $\alpha = 0.4$, $m = 0.6$, $\delta^* = 0.01$, $\Phi = 0.2$.

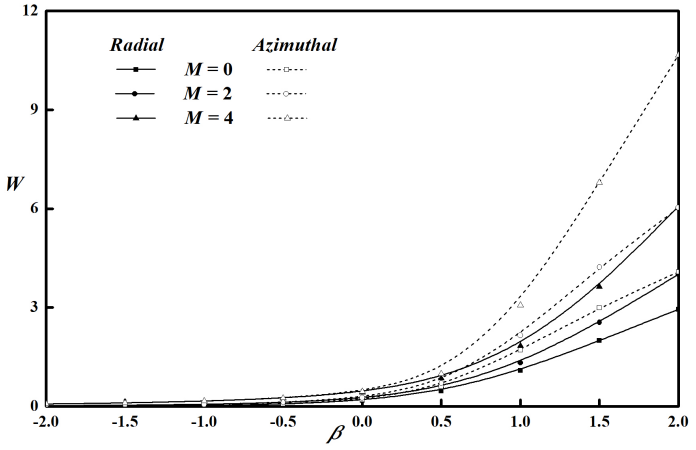

Figure 9. Variation of W against β for various values of M with $C = 0.3$, $l^* = 0.3$, $\alpha = 0.4$, $\Psi = 0.001$, $m = 0.6$, $\delta^* = 0.01$, $\Phi = 0.2$.

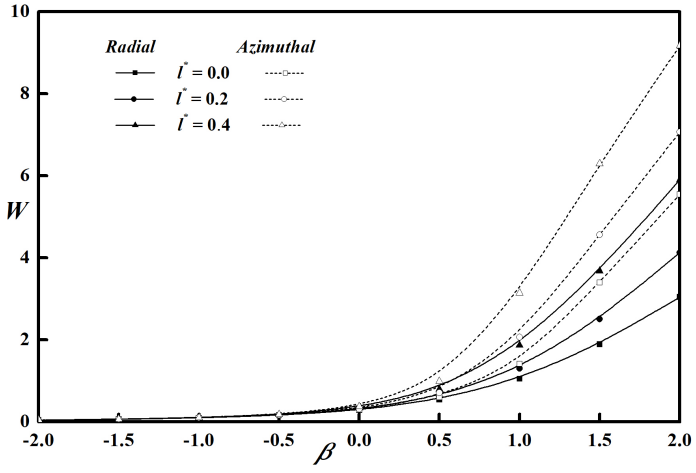

Figure 10. Variation of W against β for various values of l^* with $C = 0.3$, $M = 3$, $\alpha = 0.4$, $\Psi = 0.001$, $m = 0.6$, $\delta^* = 0.01$, $\Phi = 0.2$.

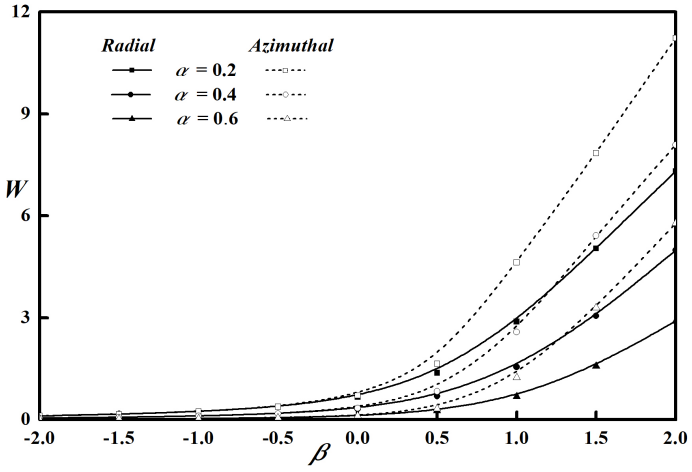

FIGURE 11. Variation of W against β for various values of α with $C = 0.3$, $M = 3$, $l^* = 0.3$, $\Psi = 0.001$, $m = 0.6$, $\delta^* = 0.01$, $\Phi = 0.2$.

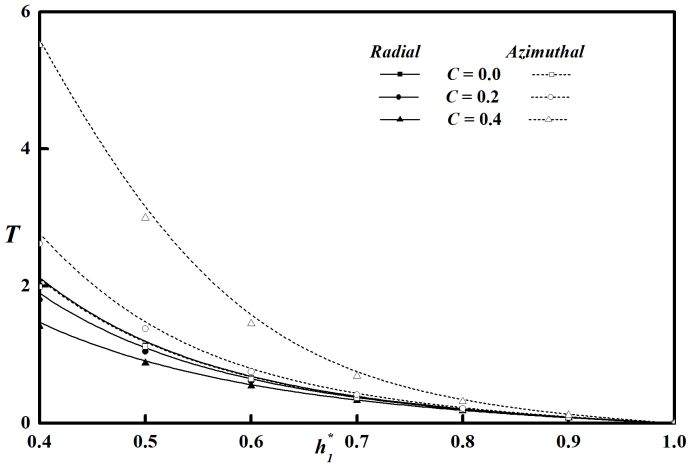

FIGURE 12. Variation of T against h_1^* for different values of C with $M = 3$, $l^* = 0.3$, $\alpha = 0.4$, $\beta = 0.5$, $\Psi = 0.001$, $m = 0.6$, $\delta^* = 0.01$, $\Phi = 0.2$.

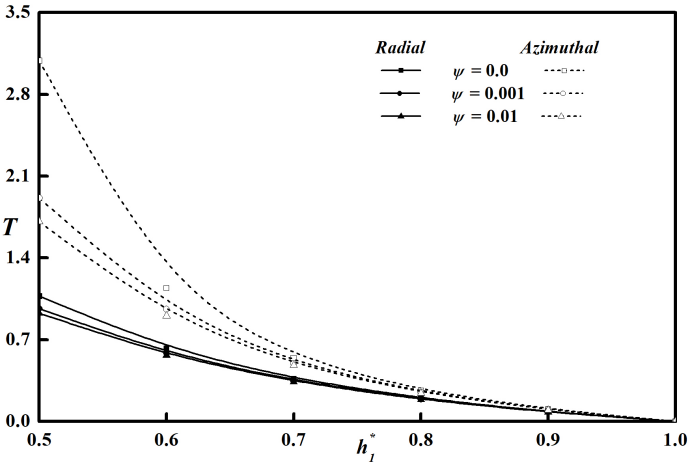

FIGURE 13. Variation of T against h_1^* for different values of Ψ with $M = 3$, $l^* = 0.3$, $C = 0.3$, $\alpha = 0.4$, $\beta = 0.5$, $m = 0.6$, $\delta^* = 0.01$, $\Phi = 0.2$.

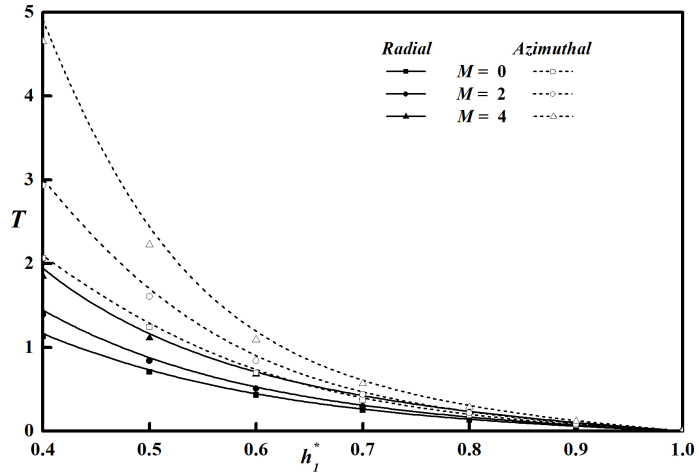

Figure 14. Variation of T against h_1^* for different values of M with $C = 0.3$, $l^* = 0.3$, $\alpha = 0.4$, $\beta = 0.5$, $\Psi = 0.001$, $m = 0.6$, $\delta^* = 0.01$, $\Phi = 0.2$.

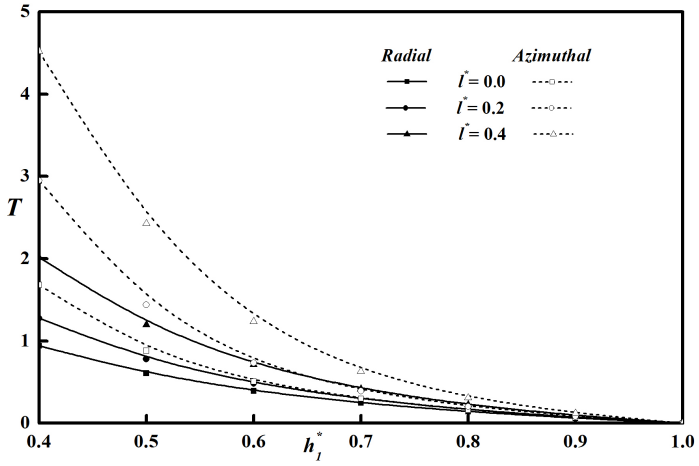

Figure 15. Variation of T against h_1^* for different values of l^* with $C = 0.3$, $M = 3$, $\alpha = 0.4$, $\beta = 0.5$, $\Psi = 0.001$, $m = 0.6$, $\delta^* = 0.01$, $\Phi = 0.2$.

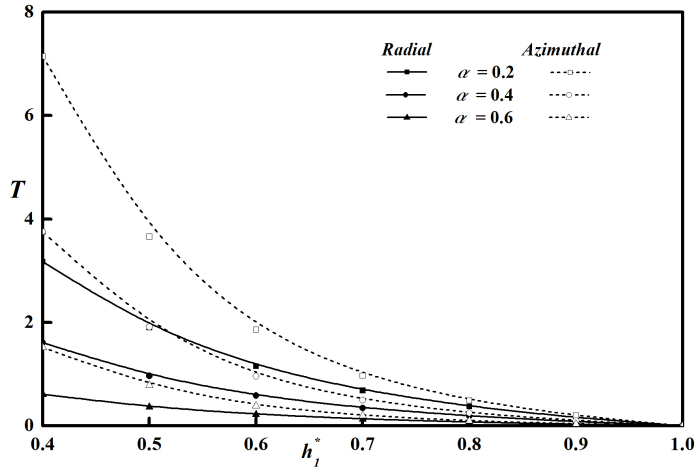

Figure 16. Variation of T against h_1^* for different values of α with $C = 0.3$, $M = 3$, $l^* = 0.3$, $\beta = 0.5$, $\Psi = 0.001$, $m = 0.6$, $\delta^* = 0.01$, $\Phi = 0.2$.

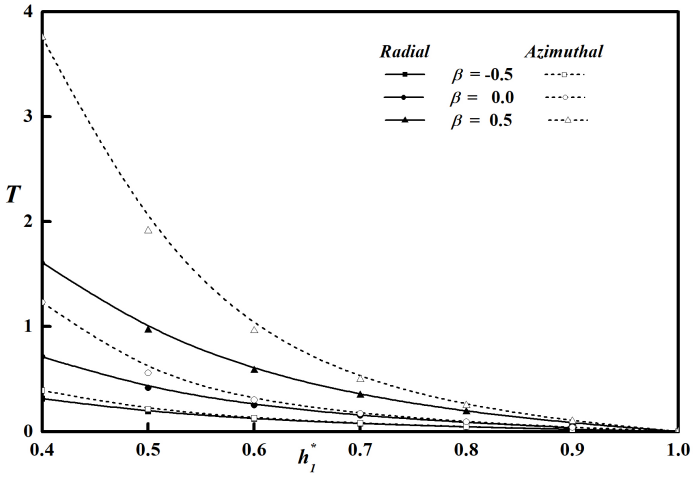

FIGURE 17. Variation of T against h_1^* for different values of β with $C = 0.3$, $M = 3$, $l^* = 0.3$, $\alpha = 0.4$, $\Psi = 0.001$, $m = 0.6$, $\delta^* = 0.01$, $\Phi = 0.2$.

	M	Hanumagowda et al. [28]		Present analysis					
				$C = 0$, $\Psi = 0$		$C = 0.2$, $l^* = 0.4$, $\Psi = 0.001$		$C = 0.2$, $l^* = 0.4$, $\Psi = 0.01$	
		$l^* = 0$	$l^* = 0.2$	$l^* = 0$	$l^* = 0.2$	Radial	Azimuthal	Radial	Azimuthal
W	0	0.3740	0.4471	0.3740	0.4471	0.5854	0.6588	0.3743	0.4016
	2	0.4610	0.5371	0.4610	0.5371	0.6946	0.7713	0.6678	0.7378
	4	0.7128	0.7980	0.7128	0.7980	0.9802	1.0591	0.9740	1.0518
	6	1.1194	1.2200	1.1194	1.2200	1.4230	1.5033	1.4201	1.5000
T	0	0.1496	0.1788	0.1496	0.1788	0.2341	0.2635	0.1497	0.1606
	2	0.1844	0.2148	0.1844	0.2148	0.2778	0.3085	0.2671	0.2951
	4	0.2851	0.3192	0.2851	0.3192	0.3920	0.4236	0.3896	0.4207
	6	0.4477	0.4880	0.4477	0.4880	0.5692	0.6013	0.5680	0.6000

TABLE 1. Numerical comparison of the Non-dimensional load carrying capacity W and Non-dimensional squeeze film time T between Hanumagowda et al. [28] and the present analysis with $h^* = 0.5$, $\beta = 0.5$, $\alpha = 0.4$, $m = 0.6$, $\delta^* = 0.01$, $\Phi = 0.2$ as fixed.

ACKNOWLEDGEMENTS

Authors acknowledge the support from REVA University for the facilities provided to carry out the research. The authors wish to express their deep gratitude to the reviewers of the original manuscript for their kind suggestions based upon which the present version of the paper has been prepared.

REFERENCES

[1] T. Ariman, M. A. Turk, N. D. Sylvester. Microcontinuum fluid mechanics – A review. *International Journal of Engineering Science* **11**(8):905–930, 1973. https://doi.org/10.1016/0020-7225(73)90038-4.

[2] T. Ariman, M. A. Turk, N. D. Sylvester. Applications of microcontinuum fluid mechanics. *International Journal of Engineering Science* **12**(4):273–293, 1974. https://doi.org/10.1016/0020-7225(74)90059-7.

[3] V. K. Stokes. Couple stresses in fluids. *The Physics of Fluids* **9**(9):1709–1715, 1966. https://doi.org/10.1063/1.1761925.

[4] J.-R. Lin. Squeeze film characteristics between a sphere and a flat plate: couple stress fluid model. *Computers & Structures* **75**(1):73–80, 2000. https://doi.org/10.1016/S0045-7949(99)00080-2.

[5] B. Kashinath. Squeeze film lubrication between parallel stepped plates with couplestress fluids. *International Journal of Statistika and Mathematika* **3**(2):65–69, 2012.

[6] N. B. Naduvinamani, A. Siddangouda. Squeeze film lubrication between circular stepped plates of couple stress fluids. *Journal of the Brazilian Society of Mechanical Sciences and Engineering* **31**(1):21–26, 2009. https://doi.org/10.1590/S1678-58782009000100004.

[7] W. T. Snyder. The magnetohydrodynamic slider bearing. *Journal of Basic Engineering* **84**(1):197–202, 1962. https://doi.org/10.1115/1.3657252.

[8] W. F. Hughes. The magnetohydrodynamic inclined slider bearing with a transverse magnetic field. *Wear* **6**(4):315–324, 1963. https://doi.org/10.1016/0043-1648(63)90164-9.

[9] W. F. Hughes. The magnetohydrodynamic finite step slider bearing. *Journal of Basic Engineering* **85**(1):129–135, 1963. https://doi.org/10.1115/1.3656508.

[10] D. C. Kuzma. The magnetohydrodynamic parallel plate slider bearing. *Journal of Basic Engineering* **87**(3):778–780, 1965. https://doi.org/10.1115/1.3650685.

[11] J.-R. Lin. Magneto-hydrodynamic squeeze film characteristics between annular disks. *Industrial Lubrication and Tribology* **53**(2):66–71, 2001. https://doi.org/10.1108/00368790110384028.

[12] J. R. Lin, R. F. Lu, W. H. Liao. Analysis of magnetohydrodynamic squeeze film characteristics between curved annular plates. *Industrial Lubrication and Tribology* **56**(5):300–305, 2004. https://doi.org/10.1108/00368790410550714.

[13] H. Christensen. Stochastic models for hydrodynamic lubrication of rough surfaces. *Proceedings of the Institution of Mechanical Engineers* **184**(1):1013–1026, 1969. https://doi.org/10.1243/PIME_PROC_1969_184_074_02.

[14] M. V. Bhat, G. M. Deberi. Squeeze film behaviour in porous annular discs lubricated with magnetic fluid. *Wear* **151**(1):123–128, 1991. https://doi.org/10.1016/0043-1648(91)90352-U.

[15] N. B. Naduvinamani, B. N. Hanumagowda, S. Tasneem Fathima. Combined effects of MHD and surface roughness on couple-stress squeeze film lubrication between porous circular stepped plates. *Tribology International* **56**:19–29, 2012. https://doi.org/10.1016/j.triboint.2012.06.012.

[16] S. T. Fathima, N. B. Naduvinamani, J. S. Kumar, B. N. Hanumagowda. Derivation of modified MHD-stochastic Reynolds equation with conducting couple stress fluid on the squeeze film lubrication of porous rough elliptical plates. *International Journal of Mathematical Archive* **5**(8):135–145, 2014.

[17] B. N. Hanumagowda, B. T. Raju, J. Santhosh Kumar, K. R. Vasanth. Combined effect of surface roughness and pressure-dependent viscosity over couple-stress squeeze film lubrication between circular stepped plates. *Proceedings of the Institution of Mechanical Engineers, Part J: Journal of Engineering Tribology* **232**(5):525–534, 2018. https://doi.org/10.1177/1350650117721432.

[18] T. Biradar, B. N. Hanumagowda, S. Biradar, et al. Effect of MHD and couple stress on squeeze film characteristics between porous curved annular circular plates. *International Journal of Mechanical and Production Engineering Research and Development* **10**(3):8535–8546, 2020.

[19] B. N. Hanumagowda, A. Salma, S. S. Nair. Combined effect of rough surface with MHD on porous conical bearing with conducting couple-stress fluid. *Palestine Journal of Mathematics* **10**(1):59–68, 2021. https://doi.org/https://pjm.ppu.edu/vol/828.

[20] J. Patel, G. M. Deheri. Influence of viscosity variation on ferrofluid based long bearing. *Reports in Mechanical Engineering* **3**(1):37–45, 2021. https://doi.org/10.31181/rme200103037j.

[21] M. Sankar, S. Kemparaju, B. M. R. Prasanna, S. Eswaramoorthi. Buoyant convection in porous annulus with discrete sources-sink pairs and internal heat generation. *Journal of Physics: Conference Series* **1139**(1):012026, 2018. https://doi.org/10.1088/1742-6596/1139/1/012026.

[22] S. Kiran, M. Sankar, Y. H. Gangadharaiah, B. V. Dhananjayamurthy. Natural convection in a linearly heated vertical porous annulus under the effect of magnetic field. In G. Manik, S. Kalia, S. K. Sahoo, et al. (eds.), *Advances in Mechanical Engineering*, pp. 537–546. Springer Singapore, Singapore, 2021. ISBN 978-981-16-0942-8, https://doi.org/10.1007/978-981-16-0942-8_50.

[23] M. E. Shimpi, G. M. Deheri. Magnetic fluid based squeeze film in rough rotating curved porous annular plates: Deformation effect. *International Journal of Mathematical and Computational Sciences* **7**(8):1370–1380, 2013. https://doi.org/10.5281/zenodo.1088604.

[24] N. C. Patel, J. R. Patel. Magnetic fluid-based squeeze film between curved porous annular plates considering the rotation of magnetic particles and slip velocity. *Journal of the Serbian Society for Computational Mechanics* **14**(2):69–82, 2020. https://doi.org/10.24874/jsscm.2020.14.02.05.

[25] J.-R. Lin, R.-F. Lu, W.-H. Liao. Analysis of MHD squeeze film characteristics between curved annular plates. *Industrial Lubrication and Tribology* **56**(5):300–305, 2004. https://doi.org/10.1108/00368790410550714.

[26] B. Kashinath, H. B. Nagangouda. MHD effect on porous wide composite slider bearing lubricated with a couplestress fluids. *Tribology Online* **10**(1):11–20, 2015. https://doi.org/10.2474/trol.10.11.

[27] V. T. Morgan, A. Cameron. Mechanism of lubrication in porous metal bearings. In *Proceedings of the Conference on Lubrication and Wear, Institution of Mechanical Engineers*, pp. 151–157. London, 1957.

[28] B. N. Hanumagowda, A. Salma. Study of squeeze film performance with MHD and couple stress between curved annular plates. *International Journal of Research and Analytical Reviews* **5**(3):669–676, 2018.

[29] J. L. Gupta, K. H. Vora. Analysis of squeeze films between curved annular plates. *Journal of Lubrication Technology* **102**(1):48–50, 1980. https://doi.org/10.1115/1.3251436.

[30] S. T. Fathima, N. B. Naduvinamani, B. N. Hanumagowda, J. S. Kumar. Modified Reynolds equation for different types of finite plates with the combined effect of MHD and couple stresses. *Tribology Transactions* **58**(4):660–667, 2015. https://doi.org/10.1080/10402004.2014.981906.

[31] A. Król, B. Giemza, T. Kałdoński. The development of the lubricants applied in the porous bearings. *Journal of KONES Powertrain and Transport* **14**(3):311–317, 2007.

A. Appendices

$$A = \left\{ \frac{1 + \left(1 - 4M^2 l^2 / h_0^2\right)^{1/2}}{2} \right\}^{1/2}$$

$$B = \left\{ \frac{1 - \left(1 - 4M^2 l^2 / h_0^2\right)^{1/2}}{2} \right\}$$

$$g_{11} = \frac{A^2}{(A^2 - B^2)} \frac{\cosh\left\{B(2z-h)/2l\right\}}{\cosh(Bh/2l)}$$

$$g_{12} = \frac{B^2}{(A^2 - B^2)} \frac{\cosh\left\{A(2z-h)/2l\right\}}{\cosh(Ah/2l)}$$

$$g_{21} = \frac{2\cosh\left\{(z-h)/\sqrt{2}l\right\} + 2\cosh\left(z/\sqrt{2}l\right)}{2\left\{\cosh\left(\sqrt{2}l\right) + 1\right\}}$$

$$g_{22} = \frac{\left(z/\sqrt{2}l\right)\sinh\left\{(z-h)/\sqrt{2}l\right\} + \left\{(z-h)/\sqrt{2}l\right\}\sinh\left(z/\sqrt{2}l\right)}{2\left\{\cosh(h/\sqrt{2}l) + 1\right\}}$$

$$g_{31} = \frac{\cos B_2 z \cosh A_2(z-h) + \cosh A_2 z \cos B_2(z-h)}{\cosh A_2 h + \cos B_2 h}$$

$$g_{32} = \frac{\cot\theta\left\{\sinh A_2 z \sin B_2(z-h) + \sin B_2 z \sinh A_2(z-h)\right\}}{\cosh A_2 h + \cos B_2 h}$$

$$A_2 = \sqrt{M/lh_0}\cos(\theta/2)$$

$$B_2 = \sqrt{M/lh_0}\sin(\theta/2)$$

$$\theta = \tan^{-1}\left(\sqrt{4l^2M^2/h_0^2 - 1}\right)$$